# Fermi surface mapping of the kagome superconductor math xmlns="http://www.w3.org/1998/Math/MathML">msub>mi>RbV/mi>mn>3/mn>/msub>msub>mi>Sb/mi>mn>5/mn>/msub>/math> using de Haas-van Alphen oscillations

Keshav Shrestha, Mengzhu Shi, Thinh Nguyen, Duncan Miertschin, Kaibao Fan, Liangzi Deng, David E. Graf, Xianhui Chen, and Ching-Wu Chu

Phys. Rev. B **107**, 075120 — Published 8 February 2023

DOI: 10.1103/PhysRevB.107.075120

# Fermi surface mapping of the kagome superconductor $RbV_3Sb_5$ using de Haas-van Alphen oscillation

Keshav Shrestha[1],* Mengzhu Shi[2], Thinh Nguyen[1], Duncan Miertschin[1], Kaibao Fan[2], Liangzi Deng[3], David E. Graf[4,5], Xianhui Chen[2], and Ching Wu Chu[3,6]

[1] *Department of Chemistry and Physics, West Texas A&M University, Canyon, Texas 79016, USA*

[2] *Hefei National Laboratory for Physical Sciences at the Microscale, University of Science and Technology of China, Hefei, 230026, China*

[3] *Texas Center for Superconductivity and Department of Physics, University of Houston, 3369 Cullen Boulevard, Houston, Texas 77204-5002, USA*

[4] *Department of Physics, Florida State University, Tallahassee, FL, 32306, USA*

[5] *National High Magnetic Field Laboratory, Tallahassee, Florida 32310, USA and*

[6] *Lawrence Berkeley National Laboratory, 1 Cyclotron Road, Berkeley, California 94720, USA*

We present the results from torque magnetometry studies of the kagome superconductor $RbV_3Sb_5$ under applied fields up to 45 T and temperatures down to liquid $^3$He temperature (0.32 K). The torque signal shows clear de Haas-van Alphen (dHvA) oscillations with eight distinct frequencies ranging from $\sim$ 150 T to 3000 T. Among these, five are above 500 T. Angle-dependent measurement of dHvA shows that all frequencies follow $1/\cos\theta$ dependence, where $\theta$ is the tilt angle with respect to the applied field direction, and the oscillations disappear above $\theta = 60^o$, which confirms that the Fermi surfaces corresponding to these frequencies are two dimensional. The Berry phase ($\phi$), calculated by constructing a Landau level fan diagram, is found to be $\sim \pi$, which strongly supports the non-trivial topology of $RbV_3Sb_5$. Using the Lifshitz-Kosevich formula, we estimate the effective mass ($m^*$) of charge carriers in $RbV_3Sb_5$, and it is found to be heavier ($\sim 0.7m_o$, where $m_o$ is the free electron mass) than that for other topological insulators. The findings of high frequencies up to 3000 T in $RbV_3Sb_5$ have not been reported previously, and the results regarding the Fermi surface of $RbV_3Sb_5$ are crucial for understanding the charge density wave order, superconductivity, and non-trivial topology in $AV_3Sb_5$ ($A$ = K, Rb, and Cs), as well as the interplay among them.

## I. INTRODUCTION

Due to their unusual lattice geometry, novel materials with a kagome lattice exhibit fascinating quantum physical phenomena, such as geometrically frustrated magnetism, non-trivial band topology, flat bands, *etc.* [1–3] Recently, the discovery of a new family of kagome materials, $AV_3Sb_5$ ($A$ = K, Rb, and Cs) [4–6], with multiple electronic orders, such as charge density wave (CDW) order, superconductivity ($T_c \sim$ 0.3 - 3 K), and non-trivial band topology has attracted enormous interest in the field of condensed matter physics. $AV_3Sb_5$ crystallizes with a hexagonal lattice of V atoms that are coordinated by Sb atoms [4, 7, 8]. The proximity of multiple Dirac points to the Fermi level [4–6] with a non-zero $Z_2$ topological invariant suggests that Dirac particles might have a dominant effect on the electrical and thermal transport of these materials. Several exotic quantum phenomena, such as CDW order near $T_{CDW} \sim$ (80 - 110 K) [7, 9–11], anomalous Hall effect (AHE) [12, 13], and van Hove singularity [14], have also been observed in this new family.

With the application of increasing external pressure, the CDW order in $AV_3Sb_5$ gradually disappears and is completely absent under a moderate pressure of 1.8 GPa, whereas superconductivity shows an unusual $M$-shaped double dome [15, 16]. These observations strongly suggest that there is an unusual interplay between the CDW order and superconductivity of $AV_3Sb_5$ requiring investigation. Detailed knowledge of the Fermi surface would be invaluable for understanding the CDW phase and superconductivity in $AV_3Sb_5$. Several Fermi surface studies [12, 13, 17–21] of these materials using both quantum oscillations and angle-resolved photoemission spectroscopy (ARPES) measurements have been reported. However, most have focused on $CsV_3Sb_5$ [19, 22–26]. Quantum oscillation frequencies up to 10 kT and a heavy effective mass ($m^*$) of the charge carriers, $m^* \sim 2m_o$, where $m_o$ is the free electron mass, were observed in $CsV_3Sb_5$. The presence of such high quantum oscillation frequencies in $CsV_3Sb_5$ is fascinating and their physical origin has yet to be explored. It has been proposed that high frequencies arise from the reconstructed Fermi surface pockets which are caused due to the CDW transition [19, 23]. Thus far, there have been limited published studies [13, 17] on other members of the $AV_3Sb_5$ family ($KV_3Sb_5$ and $RbV_3Sb_5$), in which, only low frequencies below 500 T have been reported. Using Shubnikov de-Haas (SdH) oscillations, S. Y. Yang *et al.* [13] observed two frequencies (34.6 T and 148.9 T) in $KV_3Sb_5$ and Q. Yin *et al.* [17] reported two frequencies (33.5 T and 117.2 T) in $RbV_3Sb_5$, however, detailed Fermi surface properties have yet to be reported.

Here we present the Fermiology of $RbV_3Sb_5$ using torque magnetometry with applied fields up to 45 T. The torque signal clearly shows de Haas-van Alphen (dHvA) oscillations with eight distinct frequencies up to 3000 T. Analysis of the field-angle dependence of the dHvA os-

* Corresponding e-mail: kshrestha@wtamu.edu

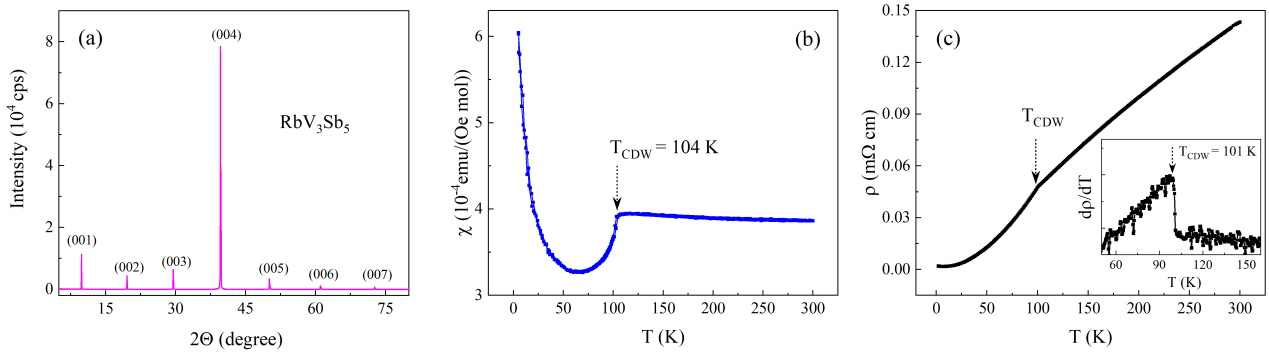


FIG. 1. **XRD, magnetic susceptibility, and electrical resistivity.** (a) Room temperature XRD pattern of a $RbV_3Sb_5$ single crystal. All peaks can be indexed to the $P6/mmm$ structure. (b) Temperature-dependent magnetic susceptibility, $\chi$ (T), of a $RbV_3Sb_5$ single crystal measured by applying $H = 7$ T along the c-axis. There is a clear jump at $T_{\rm CDW} \sim 104$ K, marked by the arrow, due to the CDW order. (c) Temperature-dependent electrical resistivity, $\rho$ (T), of a $RbV_3Sb_5$ single crystal. The $\rho$ (T) curve shows a slope change due to the CDW transition, $T_{\rm CDW} \sim 101$ K, marked by the arrow. The transition is evident in the first derivative data, as shown in the inset.

cillations, Berry phase calculation results, and Lifshitz-Kosevich (LK) analyses are also presented to completely elucidate the Fermi surface properties of this material.

## II. EXPERIMENTAL DETAILS

High-quality single crystals of $RbV_3Sb_5$ were synthesized using a self-flux method. Alkali metal Rb (99.5%), V powder (99.5%) and Sb (99.999%) were mixed at a Rb:V:Sb mole ratio of 2:1:5.2. The mixture was loaded into an alumina crucible and sealed inside a titanium container that was further sealed inside a quartz tube that was subsequently heated to 1273 K over 300 min, maintained at this temperature for 600 min, rapidly cooled down to 1173 K over 100 min, and finally slowly cooled down to 923 K over one week. The $RbV_3Sb_5$ crystals were separated from the flux using centrifugal treatment. From element analysis based on energy-dispersive X-ray (EDX) spectroscopy (Fig. S1 and Table S1 in the Supplemental Material [29]), the Rb:V:Sb atomic ratio of the obtained single-crystal $RbV_3Sb_5$ is $(0.98 \pm 0.04)$:$(3.00 \pm 0.03)$:5, is very close to the stoichiometric ratio of 1:3:5.

The crystal structure of $RbV_3Sb_5$ samples was characterized using an X-ray diffractometer (Rigaku SmartLab) equipped with Cu K$\alpha$ radiation and a fixed graphite monochromator. A field-emission scanning electron microscope (Sirion 200) was used to analyze the crystal composition through EDX and results are presented in Fig. S1 and Table S1 in the Supplemental Material [29]. Magnetic susceptibility and electrical transport measurements were carried out using a SQUID magnetometer (Quantum Design, MPMS 5 T) and a Physical Property Measurement System (Quantum Design, PPMS 9 T), respectively.

High-field measurements were carried out at the National High Magnetic Field Laboratory (NHMFL), Tallahassee, Florida, with the maximum applied fields of 41.5 T (dc resistive water-cooled magnet) and 45 T hybrid (33.5 T dc resistive magnet nested in an 11.5 T superconducting magnet) top-loaded with a $^3$He cryostat. The magnetic torque was measured using a miniature piezoresistive cantilever. A tiny $RbV_3Sb_5$ crystal was selected and then fixed to the cantilever arm with vacuum grease. The cantilever was subsequently mounted on the rotating platform of a special probe designed at NHMFL [30]. The probe was then slowly cooled down to the base temperature of 0.32 K. Two resistive elements on the cantilever were incorporated with two other room-temperature resistors to form a Wheatstone bridge, which was balanced at base temperature before taking field dependence data. The angle-dependent toque data were obtained by rotating the sample *in situ* with the applied field. Magnetic fields were swept at each fixed temperature at a rate of 2.2 T/min.

## III. EXPERIMENTAL RESULTS AND DISCUSSION

The room-temperature X-ray diffraction (XRD) pattern of $RbV_3Sb_5$ is displayed in Fig. 1(a), which shows that all peaks can be indexed to the hexagonal structure with the space group $P6/mmm$. It should be noted that there are only peaks with Miller indices $(00l,\ l = 1,\ 2,\ 3,\ldots)$, which implies that the c-axis is perpendicular to the flat surface of the crystal. Fig. 1(b) shows the temperature dependence of magnetic susceptibility, $\chi$ (T), for $RbV_3Sb_5$ measured under an applied field of 7 T along the c-axis. There exists a clear anomaly in the $\chi$ (T) data near $T_{\rm CDW} \sim 104$ K, marked by the arrow, which arises due to the CDW order [4, 6] in $RbV_3Sb_5$.

Electrical resistivity ($\rho$) *vs.* $T$ for $RbV_3Sb_5$ is shown in Fig. 1(c). $\rho$ decreases with decreasing temperature,

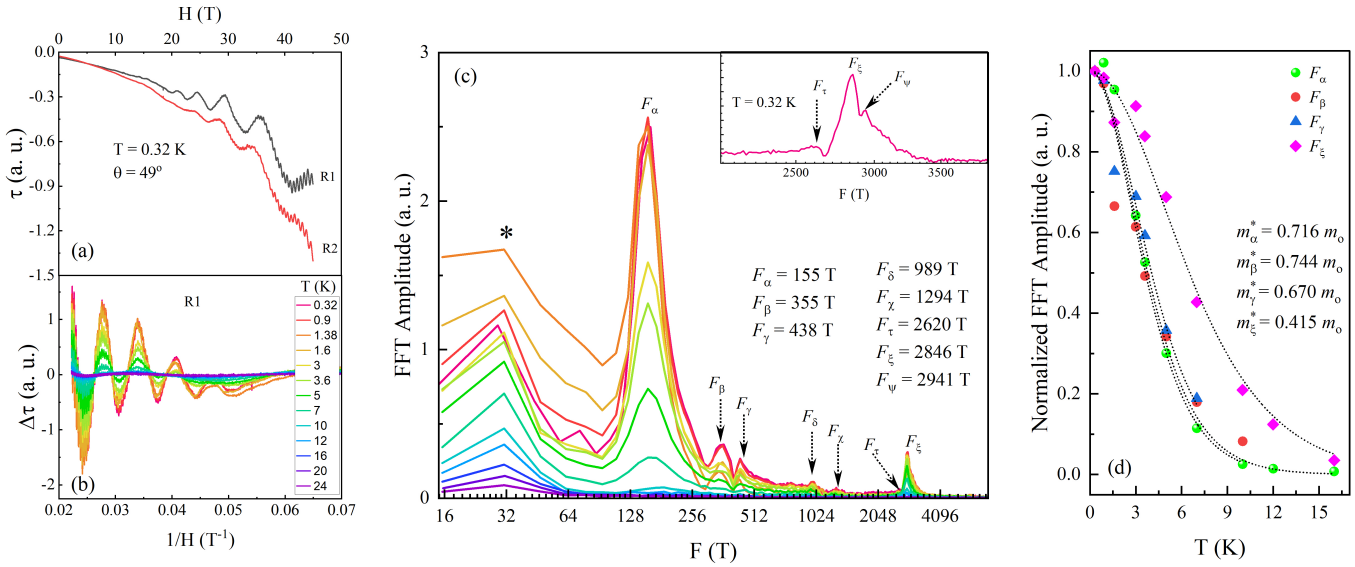


FIG. 2. **dHvA oscillations and Lifshitz-Kosevich (LK) analyses.** (a) Magnetic torque *vs.* H for two $RbV_3Sb_5$ single crystals (R1 and R2) at $\theta = 49^o$ and $T = 0.32$ K. The torque signal shows clear dHvA oscillations above 20 T. (b) Background-subtracted dHvA oscillations for R1 at different temperatures. (c) FFT spectra of background-subtracted data from (b) at different temperatures, which shows that the FFT amplitude decreases at high temperatures and that there are eight distinct peaks, five of which are above 500 T. The peak near 32 T, marked by an asterisk, is likely an artifact. The x-axis is on a logarithmic scale for better visibility of high frequencies. Inset: Magnified view of the FFT data at $T = 0.32$ K to show the highest frequencies ($F_\tau$, $F_\xi$, and $F_\psi$) more clearly. (d) Normalized FFT amplitude *vs.* $T$ for $F_\alpha$, $F_\beta$, $\gamma$, and $F_\xi$. Dotted curves: best fits using the LK formula [27, 28].

showing the compound's metallic behavior. The residual resistivity ratio (RRR) = $\rho$ (300 K)/$\rho$ (2 K) is calculated to be 73, nearly twice the value ($\sim$ 40) reported for $RbV_3Sb_5$ previously [11, 17]. Such as high RRR value confirms the excellent crystallinity of the samples studied here. The $\rho$ (T) curve in Fig. 1(c) has a slope change near $T_{\rm CDW} \sim 101$ K, marked by the arrow, which could be an indication of the CDW transition. For confirmation, we calculated the first derivative of $\rho$ (T), $d\rho/dT$, and results are shown in the inset to Fig. 1(c). The $d\rho/dT$ (T) curve has a sharp transition near $T_{\rm CDW} \sim 101$ K, marked by the arrow. The $T_{\rm CDW}$ values determined from magnetic susceptibility and resistivity measurements are thus comparable to one another and are also in close agreement with those previously reported [4, 6, 11, 17] for $RbV_3Sb_5$.

To explore the Fermi surface properties of $RbV_3Sb_5$, we measured the magnetic torque ($\tau$) under applied fields up to 45 T and temperatures down to 0.32 K. $\tau$ (H) for two single crystals (denoted as R1 and R2) of $RbV_3Sb_5$ measured at $\theta = 49^o$, where $\theta$ is the angle between the magnetic field and the c-axis of the sample, is displayed in Fig. 2(a). The amplitude of the $\tau$ signal increases with increasing $H$ and shows clear dHvA oscillations at high fields. The oscillations are observed for both R1 and R2, and frequency analyses confirm that their frequency spectra are comparable to one another (Fig. S2 in the Supplemental Material [29]). Therefore, to explore the Fermi surface properties of $RbV_3Sb_5$ here, we present the temperature and angle-dependence data for R1 only. Fig. 2(b) shows the background-subtracted torque ($\Delta\tau$) data for R1 at different temperatures. The amplitude of the oscillations decreases at high temperatures, and they completely disappear at 24 K. The oscillations appear to have multiple periods (and hence several frequencies). The frequencies of the oscillations can be determined by applying the fast Fourier transform (FFT).

Fig. 2(c) shows the FFT spectra of the background-subtracted data from Fig. 2(b) at different temperatures. As expected, there are multiple (eight) distinct peaks with values ranging from $\sim$ 150 T to 3000 T. Three frequencies ($F_\alpha = 155 \pm 25$ T, $F_\beta = 355 \pm 30$ T, and $F_\gamma = 438 \pm 22$ T) are below 500 T (denoted as low frequencies) and the remaining five ($F_\delta = 989 \pm 26$ T, $F_\chi = 1294 \pm 65$ T, $F_\tau = 2620 \pm 51$ T, $F_\xi = 2846 \pm 23$ T, and $F_\psi = 2941 \pm 15$ T) are above 500 T (denoted as high frequencies). We noticed that $F_\tau$ and $F_\psi$ are visible at low temperature, as shown in the inset to Fig. 2(c), but they disappear quickly at higher temperatures (above 5 K). To the best of our knowledge, there has been only one previously reported quantum oscillation study of $RbV_3Sb_5$, by Q. Yin *et al.* [17], who observed two low frequencies, 33.5 T and 117.2 T, in Shubnikov de-Haas (SdH) oscillations. We likewise noticed a peak near 32 T, marked by the asterisk in Fig. 2(c). Under such a high field of 45 T, it is difficult to justify the peak at 32 T as a real frequency. In addition, $F_\alpha$ changes with $\theta$ and its value is $\sim$ 110 T at $\theta = 6^o$ (see discussion below). Therefore, $F_\alpha$ is consistent with the frequency of

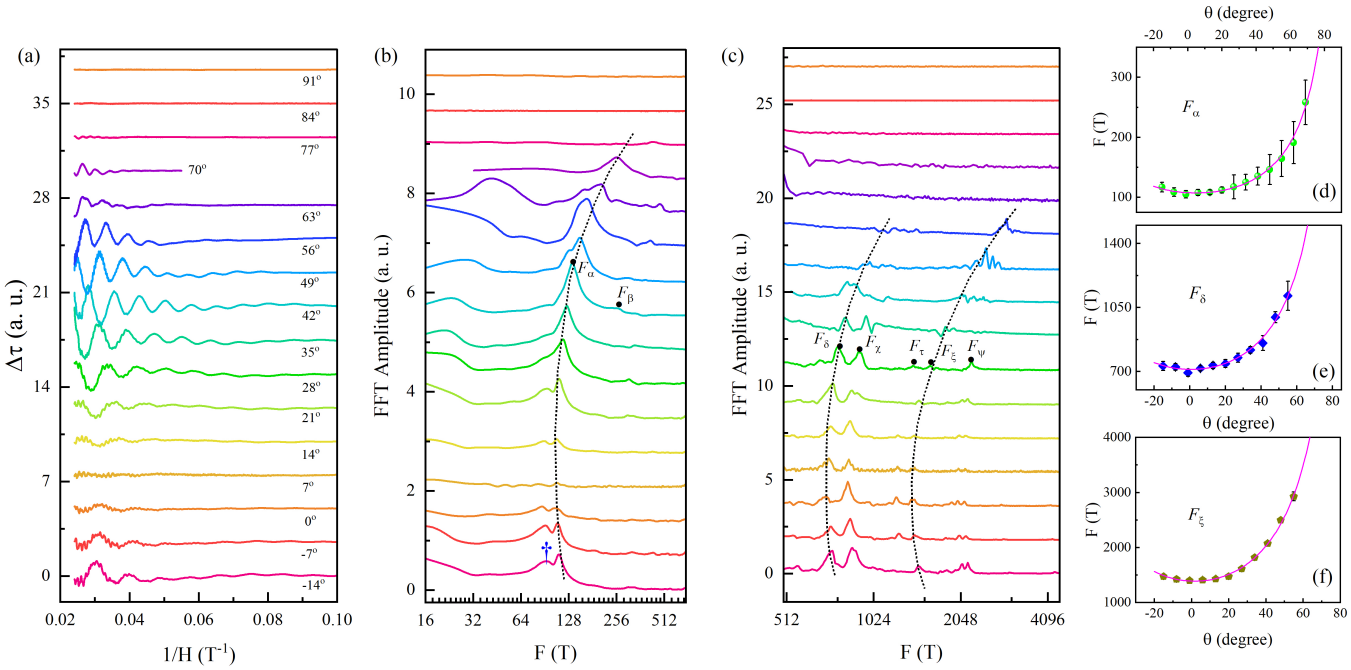


FIG. 3. **Angular dependence of quantum oscillation frequencies.** (a) Background-subtracted torque data for $RbV_3Sb_5$ at different $\theta$ values. The period (and hence the frequency) changes with $\theta$, and the oscillations are completely absent at $91^o$. FFT spectra in the ranges of (b) 0 - 550 T and (c) 500 - 5000 T. All peaks shift to the right at high angles and completely disappear above $\theta = 60^o$. The x-axes in (b) and (c) are in the logarithmic scale for better visibility of frequencies and the dotted-lines are guides for the eye. The curves in (a), (b), and (c) are shifted vertically for clarity. Angle dependence data for (d) $F_\alpha$, (e) $F_\delta$, and (f) $F_\xi$. All frequencies can be clearly resolved up to $60^o$ and they exhibit the $1/\cos\theta$ dependence (solid curves), implying that their Fermi surfaces are 2D. The error bar for each data point is defined as the half-width at half-maximum (HWHM) of the corresponding peak in the respective frequency spectrum.

117.2 T reported by Q. Yin *et al.* [17]. However, the remaining seven frequencies ($F_\alpha$, $F_\gamma$, $F_\delta$, $F_\chi$, $F_\tau$, $F_\xi$, and $F_\psi$) shown in Fig. 2(c) are novel and have never been reported previously. Our recent torque measurements of other $AV_3Sb_5$ family members ($CsV_3Sb_5$ and $KV_3Sb_5$) under high fields up to 45 T, together with results reported by other groups [19, 22–24, 31] have shown multiple quantum oscillation frequencies with values as high as 10 kT. Therefore, the observation of high frequencies in $RbV_3Sb_5$ is consistent with the findings for $KV_3Sb_5$ and $CsV_3Sb_5$, and these high frequencies might also have the same origin, *i. e.*, Fermi surface reconstruction due to the CDW order [19, 23].

As expected, the FFT amplitude decreases at higher temperatures, and this behavior can be described by the Lifshitz-Kosevich (LK) formula [27, 28]. The normalized FFT amplitude *vs.* $T$ for $F_\alpha$, $F_\beta$, $F_\gamma$, and $F_\xi$ is displayed in Fig. 2(d), which shows that the temperature-dependent FFT data can be explained by the LK formula (dotted-curves). From the best-fit parameter, we have estimated the effective mass ($m^*$) of the charge carriers for $F_\alpha$, $F_\beta$, $F_\gamma$, and $F_\xi$ to be $m^*_\alpha = (0.72 \pm 0.10)m_o$, $m^*_\beta = (0.74 \pm 0.10)m_o$, $m^*_\gamma = (0.67 \pm 0.10)m_o$, and $m^*_\xi = (0.41 \pm 0.10)m_o$, respectively. These $m^*$ values are much heavier than $m^* = 0.125m_o$ reported by Yang *et al.* [13] for $KV_3Sb_5$, and $m^* = 0.028m_o$ and $0.031m_o$ reported by Yu *et al.* [12] and $m^* = 0.06m_o$, $0.08m_o$, $0.09m_o$, and $0.11m_o$ reported by Ortiz *et al.* [19] for $CsV_3Sb_5$. However, they are comparable with $m^* \sim 0.6m_o$ reported in recent studies [22, 24–26] for $CsV_3Sb_5$.

According to Onsager's relation [27, 32, 33], the Fermi wave vector (and hence the size of the Fermi surface) is directly proportional to the quantum oscillation frequency ($F$), that is, $F = \hbar/(2e)k_F^2$, where $\hbar$ is Planck's constant and $k_F$ is the Fermi wave vector. Therefore, the presence of multiple frequencies in $RbV_3Sb_5$ with values reaching up to 3000 T implies that there exist many Fermi surface pockets with large cross-section areas in this compound. To understand the shape, size, and dimensionality of these Fermi surface pockets, we carried out angle-dependent torque measurements by rotating the sample with respect to the applied field. Fig. 3(a) shows background-subtracted torque data, $\Delta\tau$ *vs.* 1/H for $RbV_3Sb_5$ at different $\theta$ values and indicates that both the amplitude and frequencies of the oscillations appear to vary with $\theta$, the high frequencies seem to dominate only up to $63^o$, and the oscillations are completely absent above $63^o$. These findings are clearly reflected in the FFT plots, as shown in Figs. 3(b) and 3(c).

Fig. 3(b) shows that, with increasing $\theta$, $F_\alpha$ first decreases from -14$^o$ to 0$^o$, increases at higher $\theta$ values up to $70^o$, as indicated by the dotted-line guide, and disap-

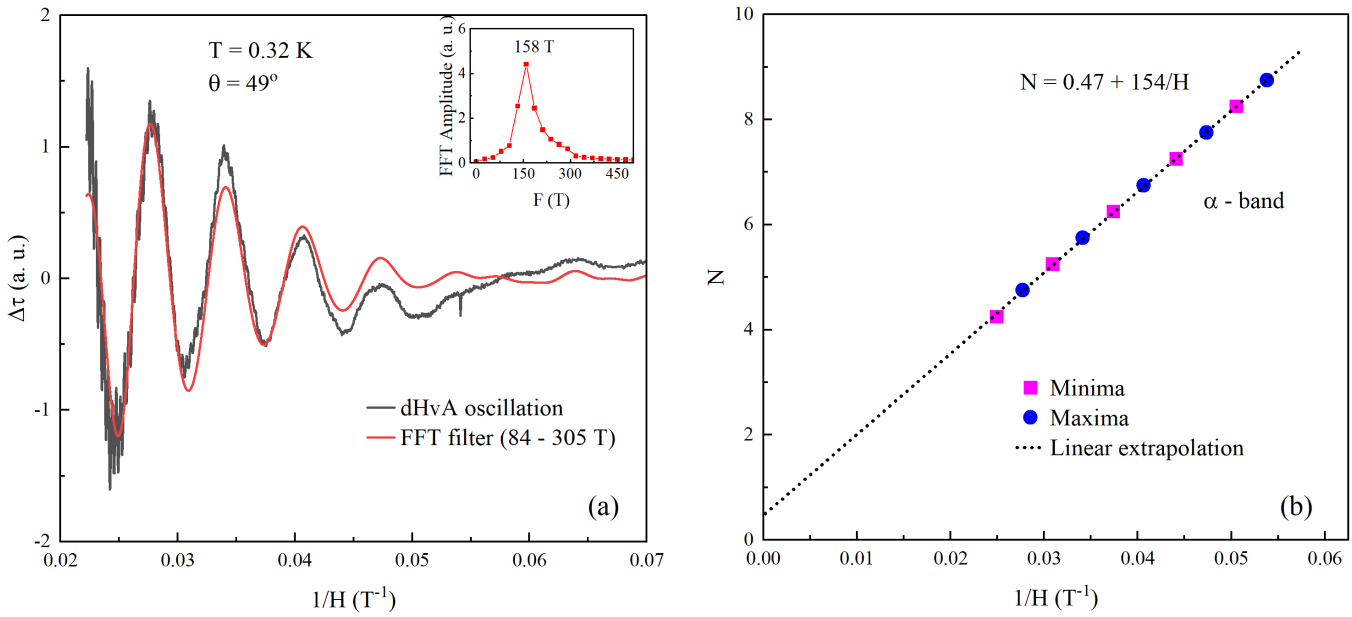


FIG. 4. **Landau level (LL) fan diagram and Berry phase.**(a) Separation of quantum oscillations for $F_\alpha$ using the band-pass filter of (84 - 305 T). Black and red curves represent the dHvA oscillation at $\theta = 49^o$ and the filtered signal, respectively. The FFT plot shows a single frequency at 158 T, as shown in the inset, confirming that the filtered signal has oscillations only for $F_\alpha$. (b) LL fan diagram for $F_\alpha$. Minima and maxima of the oscillations are assigned to $(N + 1/4)$ and $(N - 1/4)$, respectively, for constructing the LL plot. The dashed-line is the linear extrapolation of data in the limit $1/H \rightarrow 0$.

pears completely above $70^o$. Similarly, as shown in Fig. 3(c), frequencies $F_\delta$ and $F_\xi$ shift to the right at high $\theta$ before vanishing above $56^o$, as indicated by the dotted-line guides. The angular dependence of selected frequencies $F_\alpha$, $F_\delta$, and $F_\xi$ are shown in Figs. 3(d)- 3(f), respectively. As expected, these frequencies increase at high $\theta$ values and follow $1/\cos\theta$ behavior [solid curves in Fig.3(d)-3(f)]. It was found that other frequencies ($F_\chi$, $F_\sigma$, and $F_\psi$) also display $1/\cos\theta$ dependence, as shown in Fig. S3 in the Supplemental Material [29], strongly suggesting that all these frequencies originate from the two-dimensional (2D) Fermi surfaces [32, 34, 35]. The vanishing of these frequencies above $\theta = 63^o$ further supports the 2D Fermi surface origin [32, 36–38] of these frequencies. There have been a few recent reports of the existence of 2D Fermi surfaces in $CsV_3Sb_5$ [19, 22, 23, 25], and the existence of 2D Fermi surfaces in $KV_3Sb_5$ is consistent with these reports. It should be noted that there exists a peak $\sim$ 90 T, as marked by the dagger in Fig. 3(b). However, it appears only at low $\theta$ values, so we did not carry out angular dependence analyses for this frequency.

Based on the above discussion, $RbV_3Sb_5$ consists of several 2D Fermi-surface pockets. To identify the topological nature of $RbV_3Sb_5$, we calculated the Berry phase ($\phi$) by constructing a Landau level (LL) fan diagram [32, 37]. The $\phi$ values for topologically trivial and non-trivial systems are 0 and $\pi$, respectively [32, 35, 39]. However, due to the presence of multiple frequencies in the quantum oscillation data (Figs. 2 and 3), it is difficult to disentangle the oscillation corresponding to a single frequency. Therefore, we have used the band-pass filter technique [40–43] to isolate the individual frequency. The black and red curves in Fig. 4(a) represent the original torque signal and filtered data, respectively, for $RbV_3Sb_5$. There exists a single peak at 158 T in the frequency spectrum of the filtered data [see the inset to Fig. 4(a)], confirming that the filtered data has dHvA oscillations only for $F_\alpha$. It is important to note that the assignment of the LL index ($N$) for the torque data depends on the slope of the frequency *vs.* $\theta$ plot, that is, $dF/d\theta$. For a positive slope, the minima and maxima of the oscillations are assigned to $(N + \frac{1}{4})$ and $(N - \frac{1}{4})$, respectively [22, 27, 43]. As seen in Fig. 3, all the frequencies analyzed here have $dF/d\theta > 0$. Therefore, we assigned $(N + \frac{1}{4})$ and $(N - \frac{1}{4})$ for the minima and maxima, respectively, to construct the LL fan plot [Fig. 4(b)].

The value of $N_0$, obtained by a linear extrapolation of $1/H \rightarrow 0$, defines the value of the $\phi$ in units of $2\pi$. $N_0 = 0.5$ ($\phi = \pi$) is expected for Dirac particles [32, 37, 44, 45]. Here, from the linear extrapolation of the $N$ *vs.* 1/H plot in Fig. 4(b), we have obtained the intercept $N_0 = (0.47 \pm 0.04)$. This value corresponds to $\phi \sim \pi$, confirming a non-trivial Fermi surface topology of $F_\alpha$. Moreover, the linear extrapolation yields a slope equal to $(154 \pm 0.9)$ T, which is consistent with the $F_\alpha$ value of 155 T obtained from the FFT [Fig. 2(c)]. This provides evidence that (i) there is no significant error in finding the intercept (and hence the $\phi$-value) using the linear extrapolation of the $N$ *vs.* $1/H$ plot and (ii) the band-pass filter still

preserves the original dHvA oscillation signal.

We analyzed the magnetic field attenuation of the dHvA oscillations and estimated the Dingle temperature ($T_D$) of the selected frequencies, as shown in Fig. S4 in the Supplemental Material [29]. Using the experimental results for $m^*$, $T_D$, and $k_F$, we have estimated different physical parameters characterizing the Fermi surfaces of $RbV_3Sb_5$, as listed in Table 1. There exists no previously reported data on $RbV_3Sb_5$ for comparison, but these Fermi surface parameters are comparable with those for $CsV_3Sb_5$ and $KV_3Sb_5$ [22, 31].

## IV. SUMMARY

We have presented detailed information on the synthesis of $RbV_3Sb_5$, a member of the kagome superconductor family $AV_3Sb_5$ ($A$ = K, Rb, and Cs), and its Fermi surfqace characterization using torque magnetometry. The torque signal measured under a dc magnetic field of 45 T and the liquid $^3$He temperature (0.32 K) exhibit clear de Haas-van Alphen (dHvA) oscillations with multiple frequencies. There exist eight major peaks in the frequency spectrum, five of which are above 500 T. Using the temperature-dependent of quantum oscillations data, we estimated the effective mass ($m^*$) of the charge carriers in $RbV_3Sb_5$ and found that it is heavier ($m^* \sim 0.7m_o$, where $m_o$ is the free electron mass) than that of other topological insulators and Dirac/Weyl semimetals. The angular dependence of quantum oscillations allows for probing the shape and dimensionality of a Fermi surface. Here, the application of extremely high fields up to 45 T enabled us to resolve the quantum oscillation frequencies even at high tilt angles ($\theta$) up to $60^o$ and hence helped in unambiguously determining the shape of the Fermi surface. From our analyses of the field-angle data, we found that most of the frequencies observed here follow $1/\cos\theta$ dependence, which suggests that these frequencies originate from 2D Fermi surfaces. The absence of frequencies above $\theta = 60^o$ further supports the 2D nature of the Fermi surface in $RbV_3Sb_5$. The Berry phase was determined by constructing the Landau level fan diagram and found to be $\sim \pi$, strongly suggesting the non-trivial topology of $RbV_3Sb_5$. Several Fermi surface properties of $RbV_3Sb_5$ were estimated assuming a 2D Fermi surface, and those parameters are reported in Table 1.

In our previous high-field torque magnetometry studies of $CsV_3Sb_5$ and $KV_3Sb_5$ [22, 31], we reported very high quantum oscillation frequencies up to 3000 T, the presence of 2D Fermi surfaces, and heavy effective masses of charge carriers (compared to other topological systems). Therefore, our detailed high field studies of $RbV_3Sb_5$, together with our previous reports [22, 31], confirm that high quantum oscillation frequencies, relatively heavy $m^*$, 2D Fermi surfaces, *etc.* are present in all members of the $AV_3Sb_5$ compound family. The observation of high frequencies above 500 T in $AV_3Sb_5$ is quite intriguing, and these might originate from reconstructed Fermi surface pockets, as proposed previously [19, 23]. Electronic band structure and Fermi surface calculations could be helpful in explaining these high frequencies and the relatively heavy $m^*$ in $AV_3Sb_5$. The detailed Fermi surface information for $RbV_3Sb_5$ presented here will be crucial in understanding the superconductivity, charge density wave order, and topological properties of $AV_3Sb_5$.

## ACKNOWLEDGEMENTS

The work at West Texas A&M University is supported by the Killgore Faculty Research program, the KRC Undergraduate and Graduate Student Research Grants, and the Welch Foundation (Grant No. AE-0025). Work at the University of Houston was supported in part by the U.S. Air Force Office of Scientific Research Grants FA9550-15-1-0236 and FA9550-20-1-0068, the T. L. L. Temple Foundation, the John J. and Rebecca Moores Endowment, and the State of Texas through the Texas Center for Superconductivity at the University of Houston. The work at Hefei National Laboratory for Physical Sciences at the Microscale, University of Science and Technology of China is supported by the Strategic Priority Research Program of the Chinese Academy of Sciences (XDB25000000) and the National Natural Science Foundation of China (11888101). A portion of this work was performed at the National High Magnetic Field Laboratory, which is supported by National Science Foundation Cooperative Agreement No. DMR-1644779 and the State of Florida.

TABLE I. Physical parameters, including frequency ($F$), Fermi wave vector ($k_F$), Fermi surface area ($S_F$), effective mass ($m^*$), Fermi velocity ($v_F$), Dingle temperature ($T_D$), quantum relaxation time ($\tau_s$), mean free path ($l_{2D}$), and quantum mobility ($\mu$), characterizing the dHvA oscillations of $RbV_3Sb_5$.

| Band | $F$(T) | $k_F(\mathring{A}^{-1})$ | $S_F(10^{-2}$ Å$^{-2})$ | $m^*/m_o$ | $v_F(10^4$ ms$^{-1})$ | $T_D$(K) | $\tau_s(10^{-13}$s) | $l_{2D}$(nm) | $\mu(cm^2V^{-1}s^{-1})$ |
|---|---|---|---|---|---|---|---|---|---|
| $\alpha$ | 155 | 0.069 | 1.48 | 0.72 | 11.05 | 4.06 | 2.98 | 32.95 | 730.02 |
| $\beta$ | 355 | 0.104 | 3.39 | 0.74 | 16.10 | 3.60 | 3.36 | 54.12 | 792.32 |
| $\xi$ | 2846 | 0.294 | 27.14 | 0.42 | 81.73 | 15.86 | 0.76 | 62.35 | 322.42 |

[1] M. Li, Q. Wang, G. Wang, Z. Yuan, W. Song, R. Lou, Z. Liu, Y. Huang, Z. Liu, H. Lei, Z. Yin, and S. Wang, Dirac cone, flat band, and saddle point in kagome magnet ymn6sn6, Nat. Commun. **12**, 3129 (2021).

[2] M. Han, H. Inoue, S. Fang, C. John, L. Ye, M. K. Chan, D. Graf, T. Suzuki, M. P. Ghimire, W. J. Cho, E. Kaxiras, and J. G. Checkelsky, Evidence of two-dimensional flat band at the surface of antiferromagnetic kagome metal fesn, Nat. Commun. **12**, 5345 (2021).

[3] M. Kang, L. Ye, S. Fang, J.-S. You, A. Levitan, M. Han, J. I. Facio, C. Jozwiak, A. Bostwick, E. Rotenberg, M. K. Chan, R. D. McDonald, D. Graf, K. Kaznatcheev, E. Vescovo, D. C. Bell, E. Kaxiras, J. van den Brink, M. Richter, M. P. Ghimire, J. G. Checkelsky, and R. Comin, Dirac fermions and flat bands in the ideal kagome metal fesn, Nat. Mater. **19**, 163 (2020).

[4] B. R. Ortiz, L. C. Gomes, J. R. Morey, M. Winiarski, M. Bordelon, J. S. Mangum, I. W. H. Oswald, J. A. Rodriguez-Rivera, J. R. Neilson, S. D. Wilson, E. Ertekin, T. M. McQueen, and E. S. Toberer, New kagome prototype materials: discovery of kv3sb5, rbv3sb5, and csv3sb5, Phys. Rev. Mater. **3**, 094407 (2019).

[5] B. R. Ortiz, P. M. Sarte, E. M. Kenney, M. J. Graf, S. M. L. Teicher, R. Seshadri, and S. D. Wilson, Superconductivity in the z2 kagome metal kv3sb5, Phys. Rev. Mater. **5**, 034801 (2021).

[6] B. R. Ortiz, S. M. Teicher, Y. Hu, J. L. Zuo, P. M. Sarte, E. C. Schueller, A. M. Abeykoon, M. J. Krogstad, S. Rosenkranz, R. Osborn, R. Seshadri, L. Balents, J. He, and S. D. Wilson, Csv3sb5: Az2 topological kagome metal with a superconducting ground state, Phys. Rev. Lett. **125**, 247002 (2020).

[7] K. Jiang, T. Wu, J.-X. Yin, Z. Wang, M. Z. Hasan, S. D. Wilson, X. Chen, and J. Hu, Kagome superconductors av3sb5 (a=k, rb, cs), arXiv:2109.10809 (2021).

[8] T. Liang, Q. Gibson, M. N. Ali, M. Liu, R. J. Cava, and N. P. Ong1, Ultrahigh mobility and giant magnetoresistance in the dirac semimetal cd3as2., Nat. Mater. **14**, 280 (2015).

[9] F. H. Yu, D. H. Ma, W. Z. Zhuo, S. Q. Liu, X. K. Wen, B. Lei, J. J. Ying, and X. H. Chen, Unusual competition of superconductivity and charge-density-wave state in a compressed topological kagome metal, Nat. Commun. **12**, 3645 (2021).

[10] K. Y. Chen, N. N. Wang, Q. W. Yin, Y. H. Gu, K. Jiang, Z. J. Tu, C. S. Gong, Y. Uwatoko, J. P. Sun, H. C. Lei, J. P. Hu, and J. Cheng, Double superconducting dome and triple enhancement of tc in the kagome superconductor csv3sb5 under high pressure, Phys. Rev. Lett **126**, 247001 (2021).

[11] N. N. Wang, K. Y. Chen, Q. W. Yin, Y. N. N. Ma, B. Y. Pan, X. Yang, X. Y. Ji, S. L. Wu, P. F. Shan, S. X. Xu, Z. J. Tu, C. S. Gong, G. T. Liu, G. Li, Y. Uwatoko, X. L. Dong, H. C. Lei, J. P. Sun, and J.-G. Cheng, Competition between charge-density-wave and superconductivity in the kagome metal rbv3sb5, Phys. Rev. Res. **3**, 043018 (2021).

[12] F. H. Yu, T. Wu, Z. Y. Wang, B. Lei, W. Z. Zhuo, J. J. Ying, and X. H. Chen, Concurrence of anomalous hall effect and charge density wave in a superconducting topological kagome metal, Phys. Rev. B **104**, 041103 (2021).

[13] S.-Y. Yang, Y. Wang, B. R. Ortiz, D. Liu, J. Gayles, E. Derunova, R. Gonzalez-Hernandez, L. Šmejkal, Y. Chen, S. S. P. Parkin, S. D. Wilson, E. S. Toberer, and T. M. M. N. Ali, Giant, unconventional anomalous hall effect in the metallic frustrated magnet candidate, kv3sb5, Sci. Adv. **6** (2020).

[14] M. Kang, S. Fang, J. K. Kim, B. R. Ortiz, S. H. Ryu, J. Kim, J. Yoo, G. Sangiovanni, D. D. Sante, B. G. Park, C. Jozwiak, A. Bostwick, E. Rotenberg, E. Kaxiras, S. D. Wilson, J. H. Park, and R. Comin, Twofold van hove singularity and origin of charge order in topological kagome superconductor csv3sb5, Nat. Phys. **18**, 301 (2022).

[15] K. Y. Chen, N. N. Wang, Q. W. Yin, Y. H. Gu, K. Jiang, Z. J. Tu, C. S. Gong, Y. Uwatoko, J. P. Sun, H. C. Lei, J. P. Hu, and J.-G. Cheng, Double superconducting dome and triple enhancement of tc in the kagome superconductor csv3sb5 under high pressure, Phys. Rev. Lett. **126**, 247001 (2021).

[16] F. H. Yu, D. H. Ma, W. Z. Zhuo, S. Q. Liu, X. K. Wen, B. Lei, J. J. Ying, and X. H. Chen, Unusual competition of superconductivity and charge-density-wave state in a compressed topological kagome metal, Nat. Commun. **12**, 3645 (2021).

[17] Q. Yin, Z. Tu, C. Gong, Y. Fu, S. Yan, and H. Lei, Superconductivity and normal-state properties of kagome metal rbv3sb5 single crystals, Chin. Phys. Lett. **38**, 037403 (2021).

[18] K. Nakayama, Yongkai, T. Kato, M. Liu, Z. Wang, T. T. abd Yugui Yao, and T. Sato, Carrier injection and manipulation of charge-density wave in kagome superconductor csv3sb5, Phys. Rev. X **11**, 041030 (2021).

[19] B. R. Ortiz, S. M. L. Teicher, L. K. abd Paul M. Sarte, J. P. C. Ruff, R. Seshadri, and S. D. Wilson, Fermi surface mapping and the nature of charge density wave order in the kagome superconductor csv3sb5, Phys. Rev. X **11**, 041030 (2021).

[20] H. Luo, Q. Gao, H. Liu, Y. Gu, D. Wu, C. Yi, J. Jia, S. Wu, X. Luo, Y. Xu, L. Zhao, Q. Wang, H. Mao, G. Liu, Z. Zhu, Y. Shi, K. Jiang, J. Hu, Z. Xu, and X. J. Zhou, Electronic nature of charge density wave and electron-phonon coupling in kagome superconductor kv3sb5, Nat. Commun. **13**, 273 (2022).

[21] M. Kang, S. Fang, J.-K. Kim, B. R. Ortiz, S. H. Ryu, J. Kim, J. Yoo, G. Sangiovanni, D. D. Sante, B.-G. Park, C. Jozwiak, A. Bostwick, E. Rotenberg, E. Kaxiras, S. D. Wilson, J.-H. Park, and R. Comin, Twofold van hove singularity and origin of charge order in topological kagome superconductor csv3sb5, Nat. Phys. **18**, 301 (2022).

[22] K. Shrestha, R. Chapai, B. K. Pokharel, D. Miertschin, T. Nguyen, X. Zhou, D. Y. Chung, M. G. Kanatzidis, J. F. Mitchell, U. Welp, D. Popović, D. E. Graf, B. Lorenz, and W. K. Kwok, Nontrivial fermi surface topology of the kagome superconductor csv3sb5 probed by de haas–van alphen oscillations, Phys. Rev. B **105**, 024508 (2022).

[23] Y. Fu, N. Zhao, Z. Chen, Q. Yin, Z. Tu, C. Gong, C. Xi, X. Zhu, Y. Sun, K. Liu, and H. Lei, Quantum transport evidence of topological band structures of kagome superconductor csv3sb5, arXiv:2104.08193.

[24] R. Chapai, M. Leroux, V. Oliviero, D. Vignolles, M. P. Smylie, D. Y. Chung, M. G. Kanatzidis, W.-K. Kwok, J. F. Mitchell, and U. Welp, Magnetic breakdown and topology in the kagome superconductor csv3sb5 under high magnetic field, arXiv:2208.05523v2.

[25] W. Zhang, L. Wang, C. W. Tsang, X. Liu, J. Xie, W. C. Yu, K. T. Lai, and S. K. Goh, Emergence of large quantum oscillation frequencies in thin flakes of the kagome superconductor $csv_3sb_5$, Phys. Rev. B **106**, 195103 (2022).

[26] C. Broyles, D. Graf, H. Yang, X. Dong, H. Gao, and S. Ran, Effect of the interlayer ordering on the fermi surface of kagome superconductor $csv_3sb_5$ revealed by quantum oscillations, Phys. Rev. Lett. **129**, 157001 (2022).

[27] D. Shoenberg, *Magnetic Oscillations in Metals* (Cambridge University Press, 1984).

[28] K. Shrestha, V. Marinova, D. Graf, B. Lorenz, and C. W. Chu, Quantum oscillations in metallic sb2te2se topological insulator, Phys. Rev. B **95**, 075102 (2017).

[29] See Supplemental Material for detailed information regarding energy-dispersive X-ray (EDX) analyses, comparison of frequencies for samples R1 and R2, angular dependence of quantum oscillation frequencies, and Dingle temperature..

[30] E. C. Palm and T. P. Murphy, Very low friction rotator for use at low temperatures and high magnetic fields, Review of Scientific Instruments **70**, 237 (1999), https://doi.org/10.1063/1.1149571.

[31] K. Shrestha, M. Shi, T. Nguyen, D. Miertschin, K. Fan, L. Z. Deng, D. E. Graf, X. Chen, and C. W. Chu, High quantum oscillation frequencies and non-trivial topology in kagome superconductor $kv_3sb_5$ probed by torque magnetometry up to 45 t, (Manuscript under review).

[32] Y. Ando, Topological insulator materials, Phys. Rev. Mater. **5**, 034801 (2021).

[33] K. Shrestha, D. Miertschin, R. Sankar, B. Lorenz, and C. W. Chu, Large magnetoresistance and quantum oscillations in sn0.05pb0.95te, Journal of Physics: Condensed Matter **33**, 335501 (2021).

[34] D.-X. Qu, Y. S. Hor, J. Xiong, R. J. Cava, and N. P. Ong, Quantum oscillations and hall anomaly of surface states in the topological insulator $bi_2te_3$, Science **329**, 821 (2010).

[35] K. Shrestha, V. Marinova, B. Lorenz, and C. W. Chu, Evidence of a 2d fermi surface due to surface states in a p-type metallic $bi_2te_3$, J. Phys. Condens. Matt. **30**, 185601 (2018).

[36] K. Shrestha, V. Marinova, B. Lorenz, and P. C. W. Chu, Shubnikov-de haas oscillations from topological surface states of metallic $bi_2se_{2.1}te_{0.9}$, Phys. Rev. B **90**, 241111 (2014).

[37] K. Shrestha, D. E. Graf, V. Marinova, B. Lorenz, and P. C. W. Chu, Simultaneous detection of quantum oscillations from bulk and topological surface states in metallic $bi_2se_{2.1}te_{0.9}$, Phil. Mag. **97**, 1740 (2017).

[38] J. G. Analytis, R. D. McDonald, S. C. Riggs, J.-H. Chu, G. S. Boebinger, and I. R. Fisher, Two-dimensional surface state in the quantum limit of a topological insulator, Nat. Phys. **6**, 960 (2010).

[39] T. Nguyen, N. Aryal, B. K. Pokharel, L. Harnagea, D. Mierstchin, D. Popović, D. E. Graf, and K. Shrestha, Fermiology of the dirac type-ii semimetal candidates (ni,zr)te2 using de haas–van alphen oscillations, Phys. Rev. B **106**, 075154 (2022).

[40] W. Zheng, R. Schönemann, N. Aryal, Q. Zhou, D. Rhodes, Y.-C. Chiu, K.-W. Chen, E. Kampert, T. Förster, T. J. Martin, G. T. McCandless, J. Y. Chan, E. Manousakis, and L. Balicas, Detailed study of the fermi surfaces of the type-ii dirac semimetallic candidates xte2 (x=pd, pt), Phys. Rev. B **97**, 235154 (2018).

[41] W. Zheng, R. Schönemann, S. Mozaffari, Y.-C. Chiu, Z. B. Goraum, N. Aryal, E. Manousakis, T. M. Siegrist, K. Wei, and L. Balicas, Bulk fermi surfaces of the dirac type-ii semimetallic candidate nite2., Phys. Rev. B **102**, 125103 (2020).

[42] M. A. Khan, D. E. Graf, I. Vekhter, D. A. Browne, J. F. DiTusa, W. A. Phelan, and D. P. Young, Quantum oscillations and a nontrivial berry phase in the noncentrosymmetric topological superconductor candidate bipd, Phys. Rev. B **99**, 020507(R) (2019).

[43] R. Chapai, D. A. Browne, D. E. Graf, J. F. DiTusa, and R. Jin, Quantum oscillations with angular dependence in pdte2 single crystals., J. Phys.: Condens. Matter **33**, 035601 (2021).

[44] K. Shrestha, *Magnetotransport Studies on Topological Insulators* (2015).

[45] T. Nguyen, N. Aryal, B. K. Pokharel, L. Harnagea, D. Mierstchin, D. Popović, D. E. Graf, and K. Shrestha, Fermiology of the dirac type-ii semimetal candidates $(ni,zr)te_2$ using de haas–van alphen oscillations, Phys. Rev. B **106**, 075154 (2022).